Heat Capacity Study of Solution Grown Crystals of Isotactic Polystyrene

ARTICLE *in* MACROMOLECULES · JANUARY 2005

Impact Factor: 5.8 · DOI: 10.1021/ma048042l

Heat Capacity Study of Solution Grown Crystals of Isotactic Polystyrene

Hui Xu and Peggy Cebe*

Department of Physics and Astronomy, Tufts University, Medford, Massachusetts 02155

Received September 22, 2004; Revised Manuscript Received November 18, 2004

ABSTRACT: We have performed measurements of the specific heat capacity on isotactic polystyrene (iPS) crystals grown from dilute solution. Solution grown crystal (SGC) samples had larger crystal fractions and greatly reduced rigid amorphous fractions compared to their bulk cold-crystallized counterparts. Heat capacity studies were performed from below the glass transition temperature to above the melting temperature by using quasi-isothermal temperature modulated differential scanning calorimetry (TMDSC) and standard DSC. Two or three endotherms are observed, which represent the melting of crystals. The small rigid amorphous fraction relaxes in a wide temperature range from just above the glass transition temperature to just below the first crystal melting endotherm. As in bulk iPS,[1] multiple reversing melting was found in iPS SGCs, supporting the view that double melting in iPS may be due to dual thermal stability distribution existing along one single lamella.[2] The impact of reorganization and annealing on the melt endotherms was also investigated. Annealing occurs as a result of the very slow effective heating rate of the quasi-isothermal measurements compared to standard DSC. The improvement of crystal perfection through annealing causes the reversing melting endotherms to occur at a temperature higher than the endotherms seen in the standard DSC scan.

Introduction

Background. Crystals grown from dilute solution can often serve as model materials to aid in understanding the properties of their melt- or cold-crystallized counterparts. Solution grown crystals (SGCs) grow under conditions of higher molecular mobility, where the effects of chain entanglement may be reduced. Diffusion of molecules to the surface of the growing crystals is less restricted than when the polymer is crystallized by cooling from the melt or by heating from the glassy state. Thus, the number of intercrystalline tie molecules is likely to be reduced in crystals grown from dilute solution,[3] and the confining effects of crystals on the remaining amorphous phase can be minimized. In this work, the thermal properties of isotactic polystyrene (iPS) solution grown crystals are examined from below the glass transition to above the melting point. Results are compared to thermal analysis of bulk iPS cold-crystallized films reported previously,[1,4,5] in which the crystals exerted a strong confining effect on the amorphous phase.

In melt- or cold-crystallized semicrystalline polymers, the macromolecules have been recognized as being globally metastable.[6] In this view,[6] the metastable polymers have, as one characteristic property, the division into microphases and nanophases with strong, covalent bonds crossing the phase boundaries. The different phases include crystals, mesophases, glasses, and liquids.[6] The "rigid amorphous phase", or RAF,[6] is a glassy nanophase which can exist as a solid at temperatures above the glass transition temperature, T_g, of the mobile amorphous phase. In previous work on well-crystallized iPS bulk film,[1,4,5] we found that within a certain temperature range above T_g there are two solid portions, comprising the crystalline fraction (ϕ_c) and the rigid amorphous fraction (ϕ_{RAF}), and one liquid portion, the mobile amorphous fraction (ϕ_{MAF}). The mobile amorphous fraction (MAF) in iPS undergoes a typical relaxation at T_g just as it does in other semicrystalline bulk polymers, e.g., poly(ethylene terephthalate), PET,[7] poly(butylene terephthalate), PBT,[8] poly(ether ether ketone), PEEK,[9,10] poly(phenylene sulfide), PPS,[11,12] and polycarbonate, PC.[13]

In iPS bulk film, the rigid amorphous fraction was found to form at the crystallization temperature (T_c)[1] and most probably develops in parallel to the crystalline phase.[4,5] A standard DSC scan of an iPS bulk film shows three endothermic peaks. The lowest one, termed the "annealing peak", was confirmed by heat capacity measurements to be an enthalpic relaxation of RAF. This supports the point of view that the process of disordering, or devitrifying, the RAF results in an increase of enthalpy, which leads to observation of an endotherm.[6] The other two endotherms, occurring at higher temperature than the annealing peak, are due to the melting of crystals.[1] We then used quasi-isothermal temperature modulated differential scanning calorimetry (TMDSC) measurements to reveal existence of two small reversing melting peaks, each one occurring in association with one of the crystal melting endotherms seen in standard DSC. Observation of double reversing melting in iPS[1] supports Petermann's proposal that double melting peaks are due, in part, to dual thermal stability distribution along one single lamella.[2]

The existence of three phase fractions naturally increases the system's complexity, especially in the melting region. When iPS is cold crystallized at relatively higher temperatures, the relaxation of RAF (i.e., the annealing peak) overlaps with the melting of crystals and cannot be separately distinguished.[1] From this point of view, crystals grown from dilute solution constitute an ideal model to reduce the system complexity because the production of RAF is minimized by this treatment.[3] By thermal analysis of solution grown crystals, we can understand the iPS crystal melting behavior

* Corresponding author: e-mail peggy.cebe@tufts.edu.

10.1021/ma048042l CCC: $30.25
Published on Web 01/14/2005

more clearly, without the conflicting contribution from a large amount of RAF.

The earliest research on iPS solution grown crystals can be traced back to 1960−1970.[14,15] Blais et al.[14] grew iPS crystal clusters from trimethylbenzene and found the clusters consisted of flat platelets, which appeared as degenerate hexagons with serrated edges. Keith et al.[15] obtained iPS SGC with different morphologies by using different solvents. A multiple layered hexagonal structure formed in iPS grown from a polymeric solvent of atactic polystyrene. Crystallization in dimethyl phthalate (DMP) yielded a cluster of iPS SGCs. Sasaki[16] used the reaction rate theory[17,18] to determine the crystal growth rate in various solvents at different crystallization temperatures. They found that polymer−solvent interaction is a maximum in DMP solution, and the maximum growth rate occurred at about 70 °C.

We adopted the self-seeding method[15] to grow iPS SGCs in DMP to serve as model materials, which it is hoped would be relatively free of interlamellar tie molecules, and possess little or no amount of RAF. The questions we address in the present work are the following: (1) What impact does dilute solution growth of iPS crystals have on the remaining amorphous fraction? (2) Do SGCs exhibit dual reversing melting, which we observed for the first time in iPS bulk film? (3) What effect does the quasi-isothermal TMDSC treatment have on the thermal stability of solution-grown crystals of iPS?

Experimental Section

Isotactic (90%) polystyrene powder with a weight-average molecular weight of 400 000 g/mol was obtained from Scientific Polymer Products, Inc. A self-seeding technique was applied to grow iPS crystals in DMP dilute solution.[15] The iPS powder was dissolved in DMP with stirring for 20 min at 200 °C, at 0.05 wt % concentration of iPS in solvent. The homogeneous hot solution was slowly cooled to room temperature without separation of crystals. After standing for about 4 days, however, numerous small crystals precipitated. On slow heating of the suspension, all the visible crystals dissolved at about 190 °C, leaving only crystal seeds. Then the reheated homogeneous solution was quickly transferred into an oil bath to perform crystallization, where the temperature was already set to be the desired crystallization temperature (T_c). Four different temperatures have been chosen to grow crystals in DMP solution: 65, 73, 100, and 120 °C. The isothermal crystallization was carried out at each T_c for 2 weeks. Then the solution with precipitated crystals was slowly filtered at room temperature under slight suction to form a mat. The crystal mats were rinsed and washed with methanol several times to remove residual DMP. Finally, the SGC sample was dried in a vacuum oven for 24 h at room temperature.

The infrared spectra of iPS SGC mats were obtained in transmission mode with a Bruker Equinox Fourier transform infrared spectrometer. The resolution was 4 cm^{-1}, and 64 scans were coadded to obtain a spectrum of each sample. To evaluate the molecular chain conformation, the IR spectrum of a well-crystallized iPS bulk film was also taken for comparison. Here, "well-crystallized" refers to a film that has been crystallized to completion and displays no exothermic heat flow when cooled from the crystallization temperature.

A TA Instruments temperature-modulated DSC (TA 2920 MDSC) was used for standard DSC and quasi-isothermal TMDSC measurements. Cooling was accomplished by a TA Instruments liquid nitrogen cooling accessory (LNCA). Dry nitrogen gas was purged into the TMDSC cell with a flow rate of 20 mL/min. The temperature of the TMDSC instrument was initially calibrated in the standard DSC mode by using the onset of the melting peak for indium at a heating rate of 10 °C/min. Heat flow amplitude calibration was performed for standard DSC and quasi-isothermal TMDSC. Complete details of the calibration procedure are provided in ref 1. The sapphire, indium, and iPS SGC samples were encapsulated in Al pans. In our thermal analysis figures, except where noted, the heat capacity endotherms are presented with upward deflection from the baseline. The degree of crystallinity was determined from the area of the DSC endotherms with a sigmoidal baseline, using $\Delta H^\circ_f = 86.6$ J/g as the heat of fusion of 100% crystalline iPS.[19]

Standard DSC was carried out with a heating rate of 10 °C/min from room temperature to 260 °C. Three runs were taken to determine the sample heat capacity. The first run is empty Al sample pan ($m = 22.80$ mg) vs empty Al reference pan ($m = 17.67$ mg) to obtain baseline correction. The second run is sapphire standard vs empty Al reference pan to calibrate heat flow amplitude.[1] The third run is sample vs empty Al reference pan. The same empty Al reference pan ($m = 17.67$ mg) was used in all the runs, and all the Al sample pans were kept the same in weight ($m = 22.80$ mg). The sample mass was kept at about 10 mg.

Standard DSC was used to determine the amount of mobile amorphous fraction, ϕ_{MAF}, from the ratio of heat capacity increments at the glass transition according to[20]

$$\phi_{MAF} = \Delta C_p^{SC}/\Delta C_p^{AM} \quad (1)$$

where ΔC_p^{AM} is the heat capacity increment at the glass transition of 100% amorphous material, while ΔC_p^{SC} is the experimentally measured heat capacity increment at the glass transition for the semicrystalline polymer. In a three-phase model, the rigid amorphous fraction (RAF) makes no contribution to the heat capacity increment at T_g. The amount of the rigid amorphous fraction is obtained from $\phi_{RAF} = 1 - \phi_c - \phi_{MAF}$.

The reversing heat capacity measurement of quasi-isothermal TMDSC also consisted of three runs. The first run is empty Al sample pan vs empty Al reference pan to obtain the cell asymmetry correction.[1,21] The second run is sapphire standard vs empty Al reference pan to calibrate heat flow amplitude. The third run is sample vs empty Al reference pan. As before, the same empty Al reference pan ($m = 17.67$) was used in all the runs, and all the Al sample pans were kept the same in weight ($m = 22.80$ mg). The Al sample pan was over weighted by 5.13 mg compared to the reference pan to maintain the same cell asymmetry ($\Delta m = 5.13$ mg). The quasi-isothermal TMDSC experiment was carried out at temperature, T_0, over the temperature range of 60−270 °C with a stepwise temperature increase of 2 °C. Because of the limited capacity of liquid nitrogen in our LNCA, we can only achieve 32 temperature steps of 20 min duration before exhausting the liquid nitrogen. Therefore, the whole temperature range from 60 to 270 °C was separated into four parts. Our experimental results showed that this method introduced no uncertainty. The temperature modulation amplitude is 0.5 °C, and the oscillation period is 1 min. Each quasi-isothermal run lasted 20 min, and the heat capacity at given T_0 was calculated by averaging the data points collected during the last 10 min. The appearance of the Lissajous figure was used to verify that the steady state was achieved.[1]

Results

FTIR Spectroscopy. Figure 1 shows the FTIR spectrum of an iPS SGC sample crystallized at $T_c = 100$ °C (upper solid curve) and a well-crystallized iPS bulk film crystallized at $T_c = 170$ °C for 4 h (lower dashed curve). Band assignments are based on literature, and several bands are marked with lines and their corresponding vibrational frequencies.[22−28] Compared to the bulk film, the spectrum of the SGC sample shows similarly strong absorption at 566, 586, 620, 896, 920, 1050, 1081, 1185, 1197, and 1327 cm^{-1}. According to

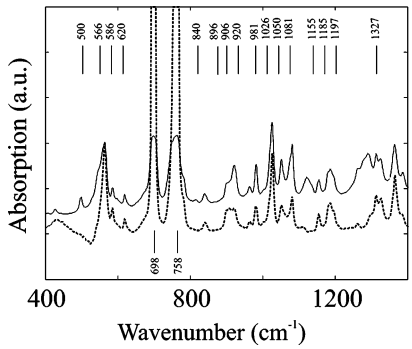

Figure 1. FTIR spectrumof an iPS SGC sample crystallized at 100 °C (upper solid curve) and an iPS well-crystallized bulk sample, cold crystallized at 170 °C for 4 h (lower dashed curve).

the literature, those bands are characteristic $(TG)_3$ helix bands, and this indicates that the molecular chain conformation in our iPS SGC sample is the $(TG)_3$ helical structure. Furthermore, the amorphous bands at 840, 906, and 1155 cm^{-1} are apparent in the SGC sample, and their relative intensities are similar to that seen in the well-crystallized bulk sample. This suggests that there is comparable amount of amorphous molecules in our SGC mat samples. The band at 698 cm^{-1} is attributed to the out-of-plane bending mode of the phenyl C−H.[27] The band height reduction at 698 and 758 cm^{-1} in the SGC sample is possibly due to the difference of the condensed state of iPS SGCs compared to bulk film.[27]

In our previous work,[4] we determined the correlation between band intensity ratio, $I_{(981\ cm^{-1})}/I_{(1026\ cm^{-1})}$, and crystallinity, since the crystalline band at 981 cm^{-1} is very sensitive to crystal growth and the band at 1026 cm^{-1} can serve as an internal standard.[24,26] The correlation equation is

$$I_{(981\ cm^{-1})}/I_{(1026\ cm^{-1})} = 0.54\phi_c + 0.16 \qquad (2)$$

In Figure 1, one can see that the 981 cm^{-1} band in the SGC sample is stronger than in the bulk sample. From eq 2 we find that the degree of crystallinity of the SGC sample grown at 100 °C is about 0.50, which is about 0.10 greater than the crystallinity of a well-crystallized bulk film. The spectra of SGC samples grown at other T_c's were also collected, but since they show very similar features, we do not present them here. The degrees of crystallinity for the other three samples (T_c = 120, 65, and 73 °C), listed in Table 1, are similar, with a variation of about 0.03−0.04. Since the crystal growth rate in DMP solution is maximum at about T_c = 70 °C,[16] the SGC samples crystallized at the lower T_c's (either T_c = 65 °C or T_c = 73 °C) have a slightly greater crystallinity than the samples grown at the higher T_c's.

Heat Capacity Using Standard DSC. Figure 2a−d shows the specific total heat capacity from standard DSC scans of iPS SGC samples, which were crystallized for 12 h at T_c = 65, 73, 100, and 120 °C, respectively. Figure 2e shows a standard DSC scan of a well-crystallized iPS bulk film for comparison. The heating rate is 10 K/min, and the sample mass is about 10 mg. In Figure 2a, the glass transition temperature and melting endotherms of SGC samples are marked. At higher temperature in the DSC scan, two or three endotherms are observed depending on the crystallization temperature. As shown in Figure 2, we assign the lowest endothermic peak as T_{m1}, the uppermost endotherm as T_{m2}, and the shoulder located at a temperature a little bit lower than T_{m2} as T_{mr}. The values of T_g, T_{m1}, T_{m2}, and T_{mr} are listed in Table 1.

In Figure 3, we plot T_g (○), T_{m1} (□), T_{m2} (△), and T_{mr} (◇) against crystallization temperature, T_c. T_g, T_{m1}, and T_{mr} have a relatively stronger dependence on T_c, shifting to higher temperatures when T_c was increased. T_{mr} is always located about 30 deg above T_{m1}. The uppermost endotherm, T_{m2}, has slight dependence on T_c. The line $T_{m2} = T_c$ is also shown for comparison, and for our four data points the extrapolation to the infinite crystal melting point occurs at 509 K (236 °C). The literature value of T_m^0 is 515 K (242 °C).[29]

Since the iPS crystals grown from solution and iPS bulk film crystallized from the glassy state are different systems, there is no direct comparison of melting temperature between them. However, it seems the uppermost melting temperatures (T_{m2}) in both systems have a similar independence of crystallization temperature. The reason why T_{m2} of the SGC sample has a lower value than T_{m2} of the iPS bulk sample could possibly be explained by the initial crystal perfection (stability) effect. The SGCs have relatively lower crystal perfection than their bulk cold crystallized iPS counterparts.

In the standard DSC scans, the glass transition was found at about 385−393 K (112−120 °C) for different SGC samples. These glass transition temperatures, listed in Table 1, are higher than the typical T_g of well-crystallized bulk iPS film (shown in Figure 2e), which is about 377 K (104 °C).[1,4,5] In addition, we observe that there is little change in the low-temperature starting point of the glass transition region compared to well-crystallized bulk film. The effect of the SGCs is to shift both the inflection point and the ending point of the glass transition region to higher temperatures, an effect that is seen most strongly in the SGC samples crystallized at 100 and 120 °C. These two SGC samples also show a still measurable, but small, amount of RAF. Strong interaction across the interface between the amorphous and crystalline phases will result in an increase of the upper end of the glass transition.[31] The reason why the SGC samples show a high T_g, while at the same time minimizing the formation of RAF, is under further investigation.

In Figure 4, we show an expanded view of the specific total heat capacity from standard DSC scans of iPS SGC samples, which were shown in wide scaling in Figure 2a−d. The dashed line is the heat capacity of liquid iPS, and the dotted line is the heat capacity of solid iPS obtained from the ATHAS data bank.[30] These lines from the ATHAS data bank exactly matched our experimentally measured solid and liquid heat capacities.

In general, the baseline heat capacity is given as

$$C_p^{baseline}(T) = C_{p,solid}(T)\phi_{solid} + C_{p,liquid}(T)\phi_{liquid} \qquad (3)$$

The values of $C_{p,solid}$ and $C_{p,liquid}$ are taken from the ATHAS data bank. We now consider models for the baseline heat capacity in the temperature range from T_g up to T_{m1}. Over this restricted temperature range, there is no melting of the crystal fraction. Our purpose is to explore the possibility of the relaxation of the RAF within this temperature range. Prior to the relaxation of the RAF (and before any crystals melt), the baseline

Table 1. Parameters Characterizing IPS Crystals as a Function of Crystallization Temperature: Weight Fractions of Crystal, Mobile Amorphous and Rigid Amorphous Phases, Glass Transition, and Melting Peak Temperatures

	ϕ_c[a] (±0.01)							
T_c (°C)	DSC	FTIR	ϕ_{MAF}[b] (±0.01)	ϕ_{RAF}[c] (±0.01)	T_g (K) (±0.5)	T_{m1} (K) (±0.5)	T_{mr} (K) (±0.5)	T_{m2} (K) (±0.5)
65[d]	0.54	0.53	0.46	<0.01	385	442	473	489
73[d]	0.55	0.54	0.45	<0.01	388	451	480	490
100[d]	0.49	0.48	0.49	0.02	391	468		492
120[d]	0.47	0.47	0.50	0.03	393	478		493
bulk iPS[e]	0.40	0.39	0.50	0.10	377	477		495

[a] Determined from DSC endotherm area and FTIR band ratio. [b] Determined from the heat capacity step at the glass transition using eq 1. [c] Determined from $\phi_{RAF} = 1 - \phi_c - \phi_{MAF}$. [d] iPS crystals grown in dimethyl phthalate for 2 weeks, at concentration of 0.05wt % iPS in DMP. Conversion to kelvin can be accomplished by adding 273.15 to the temperatures in celsius. [e] Bulk iPS sample cold-crystallized at 170 °C for 4 h.[1]

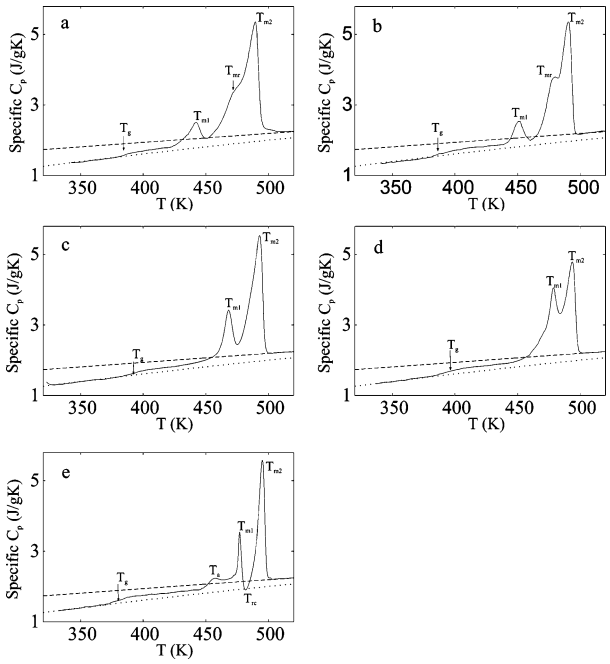

Figure 2. Specific heat capacity (wide scaling) vs temperature from standard DSC scans of iPS SGC samples crystallized at different T_c (a−d) and well-crystallized bulk iPS film (e) at a heating rate of 10 K/min. Specific heat capacity of liquid iPS (dashed line) and solid iPS (dotted line) are from the ATHAS data bank.[30] (a) SGC, $T_c = 65$ °C; (b) SGC, $T_c = 73$ °C; (c) SGC, $T_c = 100$ °C; (d) SGC, $T_c = 120$ °C; (e) cold-crystallized iPS bulk film, $T_c = 170$ °C, for 4 h.

heat capacity under a three-phase model assumption will be given by

$$C_p^{\text{baseline, 3phase}}(T) = C_{p,\text{solid}}(T)(\phi_c + \phi_{RAF}) + C_{p,\text{liquid}}(T)\phi_{MAF} \quad (4)$$

where the phase fractions take the values listed in Table 2 for the three-phase model. The baseline heat capacity, $C_p^{\text{baseline, 3phase}}(T)$, is determined on the assumption that none of the individual phase fraction changes over the temperature range.

On the other hand, if the RAF relaxes to become liquid MAF, our sample would comprise only two phases, such that $\phi_{solid} = \phi_c$ and $\phi_{liquid} = 1 - \phi_c$. The phase fractions under a two-phase model assumption are also listed in Table 2. The baseline heat capacity between the T_g and the lowest endotherm T_{m1} would be expressed using a two-phase model by setting $\phi_{RAF} = 0$ in eq 4.

Within experimental error, there is practically no RAF in the SGC samples crystallized at 65 or 73 °C.

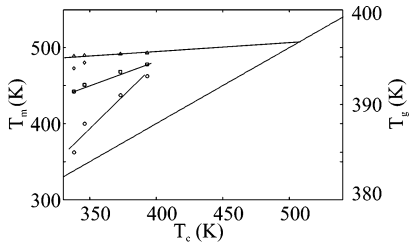

Figure 3. Crystallization temperature dependence of the glass transition temperature (right-hand vertical axis) and melting temperatures, T_{m1} and T_{m2}, and recrystallization temperature, T_{rc} (left-hand vertical axis): T_g (○), T_{m1} (□), T_{m2} (△), and T_{mr} (◇). The lines with symbols are guides to the eye and represent the best fits to the data set. The line without symbols is the line $T_m = T_c$.

For these samples, the two-phase model, setting $\phi_{RAF} = 0$ in eq 4, produces a baseline heat capacity indicated by the blue line in Figure 4a,b. In samples crystallized at 100 or 120 °C, a small amount of RAF was found, about 0.02−0.03. For these two samples, two solid lines are drawn in Figure 4c,d, which represents the baseline heat capacity under a three-phase (red solid line) or a two-phase (blue solid line) assumption. The blue solid line thus refers to the situation in which the RAF has relaxed to join the already-mobile MAF, while the crystals are unaffected. The intersection of the red solid line (three-phase model) and the experimental heat capacity trace, marked with a red arrow, reflects the end of the glass transition region and the start of the relaxation of the RAF. The intersection of the blue solid line (two-phase model) and the experimental heat capacity trace, marked with a blue arrow, reflects the end of the relaxation of RAF and the start of the crystal melting region where the temperature-dependent crystallinity, $\phi_c(T)$, begins to decrease.

As shown in Figure 4c,d, above the glass transition, for SGC samples crystallized at $T_c = 100$ and 120 °C, the total heat capacity trace does not match the baseline heat capacity based on the three-phase model (red solid line). There is always excess heat capacity above T_g and below T_{m1}, i.e., the total heat capacity trace crosses over first the red line at the red arrow (three-phase model) and then the blue line at the blue arrow (two-phase model). As will be described later when Figure 7 is discussed, just above T_g deviations also exist between the specific total heat capacity and the baseline, quasi-isothermal TMDSC reversing heat capacity. This result provides further support for the idea that an irreversible, enthalpy-producing event occurs above T_g, which is possibly due to relaxation of rigid amorphous fraction (RAF). In SGC samples, the RAF relaxes gradually in a wider temperature range than was observed for RAF relaxation in bulk iPS films.[1] After crystallization was

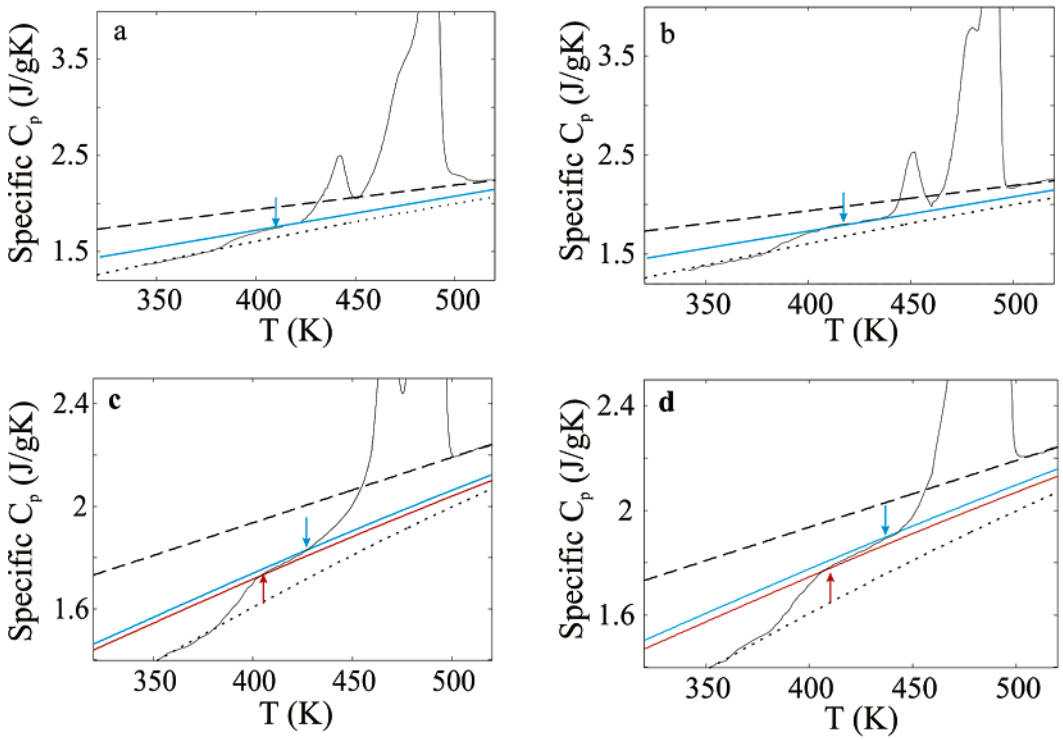

Figure 4. Specific heat capacity (expanded scaling) vs temperature from standard DSC scans of iPS SGC samples crystallized at different T_c, at a heating rate of 10 K/min. Specific heat capacity of liquid iPS (dashed line) and solid iPS (dotted line) are from the ATHAS data bank.[30] The solid lines refer to three-phase model (red line) or two-phase model (blue line) baselines having the phase fractions listed in Table 2. The intersections of the baselines and the experimental curves are marked with colored arrows (red for the intersection of the three-phase model baseline and blue for the intersection of the two-phase model baseline). (a) T_c = 65 °C; (b) T_c = 73 °C; (c) T_c = 100 °C; (d) T_c = 120 °C.

Table 2. Model Parameters Characterizing IPS SGC Samples Grown at the Indicated Temperatures: Crystal, Mobile Amorphous, and Rigid Amorphous Fractions under Three-Phase or Two-Phase[a] Model Assumptions

	three-phase model			two-phase model		
T_c (°C)	ϕ_c[b]	ϕ_{MAF}[c]	ϕ_{RAF}[d]	ϕ_c[b]	ϕ_{MAF}[e]	ϕ_{RAF}
65[f]	0.54	0.46	0	0.54	0.46	0
73[f]	0.55	0.45	0	0.55	0.45	0
100	0.49	0.49	0.02	0.49	0.51	0
120	0.47	0.50	0.03	0.47	0.53	0

[a] Two-phase model is based on an assumption that all RAF has relaxed, so that $\phi_{RAF} = 0$. [b] Determined from the crystalline fractions derived from DSC endotherm area and FTIR band ratio. [c] Determined from the heat capacity step at the glass transition according to eq 1. [d] $\phi_{RAF} = 1 - \phi_c - \phi_{MAF}$. [e] $\phi_{MAF} = 1 - \phi_c$. [f] The small amount of RAF in these samples results in identical three- or two-phase model parameters.

finished at T_c = 100 and 120 °C, the solution with crystals was cooled to room temperature, and we suspect that the RAF forms during this cooling process.

To study the origin of the small excess heat capacity above the glass transition, the following experiment was performed. We took iPS SGC samples grown at high T_c (100 and 120 °C) and heated them in the Mettler hot stage to 423 K (150 °C, for T_c = 100 °C) or 430 K (157 °C, for T_c = 120 °C) at 10 K/min and then quenched them into liquid nitrogen. The processed samples were transferred to the DSC cell after being sealed in Al pans, and standard DSC scan with heating rate of 10 K/min was performed. In Figure 5a–d, scans of the original sample (red solid curve) and treated sample (blue solid curve) are displayed. In Figure 5, parts a and b refer to T_c = 100 °C, while parts c and d refer to T_c = 120 °C. The red solid curve is the scan of original sample; the blue solid curve is the scan of the treated sample. The dashed line is the heat capacity of iPS liquid; the dotted line is the heat capacity of iPS solid from the ATHAS data bank.[30] The baseline heat capacity above T_g has been calculated assuming two different phase fractions for solid phase and liquid phases. In Figure 5a,b, the red solid line is the baseline heat capacity based on the three-phase model; the blue solid line is the baseline capacity based on the two-phase model. Phase fractions are listed in Table 2.

Some important features are demonstrated in Figure 5. First, the original samples (red curve) and treated samples (blue curve) have almost the same melting points, T_{m1} and T_{m2}, and endotherm areas, so the treatment changed the properties of the original crystals by a small amount. The melting range of the treated samples (blue curve) is slightly narrower than that of the original samples (red curve), which is explained by annealing (perfecting) of the least perfect crystals that originally melted in the lower temperature tail of endotherm T_{m1}. Second, the glass transition moves to a *lower* temperature after the treatment, becoming comparable to values of T_g seen in well-crystallized iPS bulk films.

Third, above the glass transition, the specific total heat capacity of the treated sample (blue curve) returns to the two-phase model baseline (blue solid line) with a small decrease of solid fraction. Given the error range on the measurements, the decrease of solid fraction ranges from about 0.02 to 0.03. These observations support the view that the small amount of RAF in these two samples possibly causes the high glass transition temperature as well as the excess heat capacity seen above T_g. Once the temperature increases briefly, the

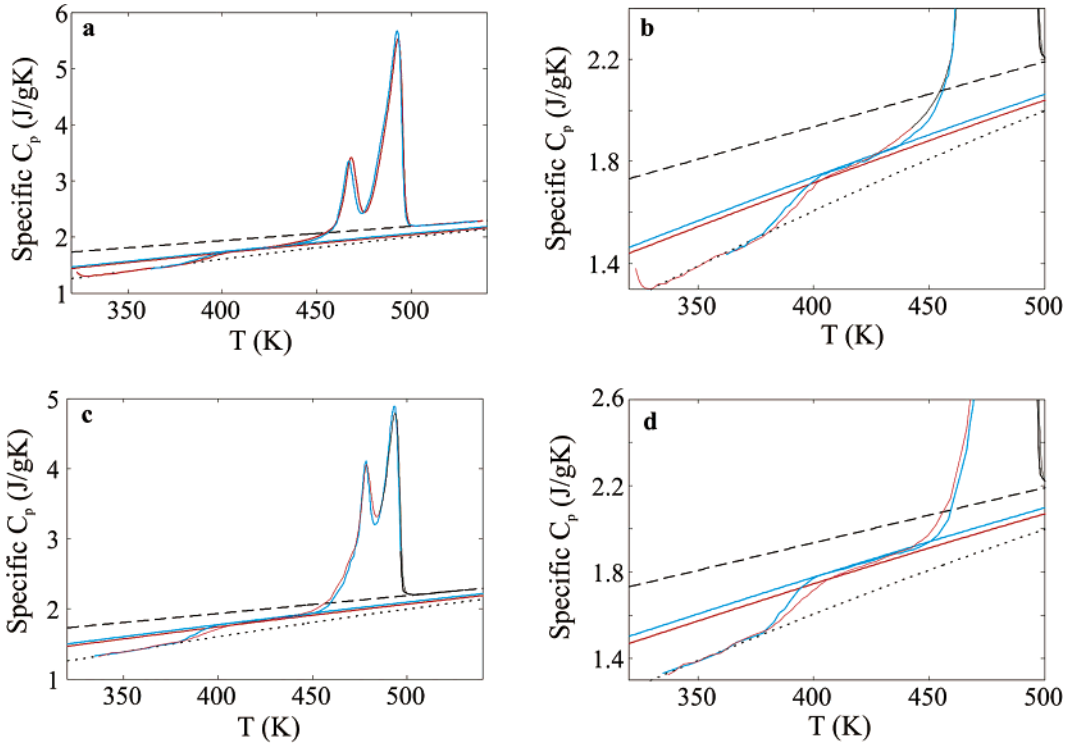

Figure 5. Comparison of standard DSC scans of original iPS SGC samples (red solid curves) and treated samples (blue solid curves) crystallized at different T_c. Specific heat capacity of liquid iPS (dashed line) and solid iPS (dotted line) are from the ATHAS data bank.[30] The solid lines refer to three-phase model (red solid line) or two-phase model (blue solid line) baselines with phase fractions listed in Table 2. (a) T_c = 100 °C, wide scaling; (b) expanded scaling of (a); (c) T_c = 120 °C, wide scaling; (d) expanded scaling of (c).

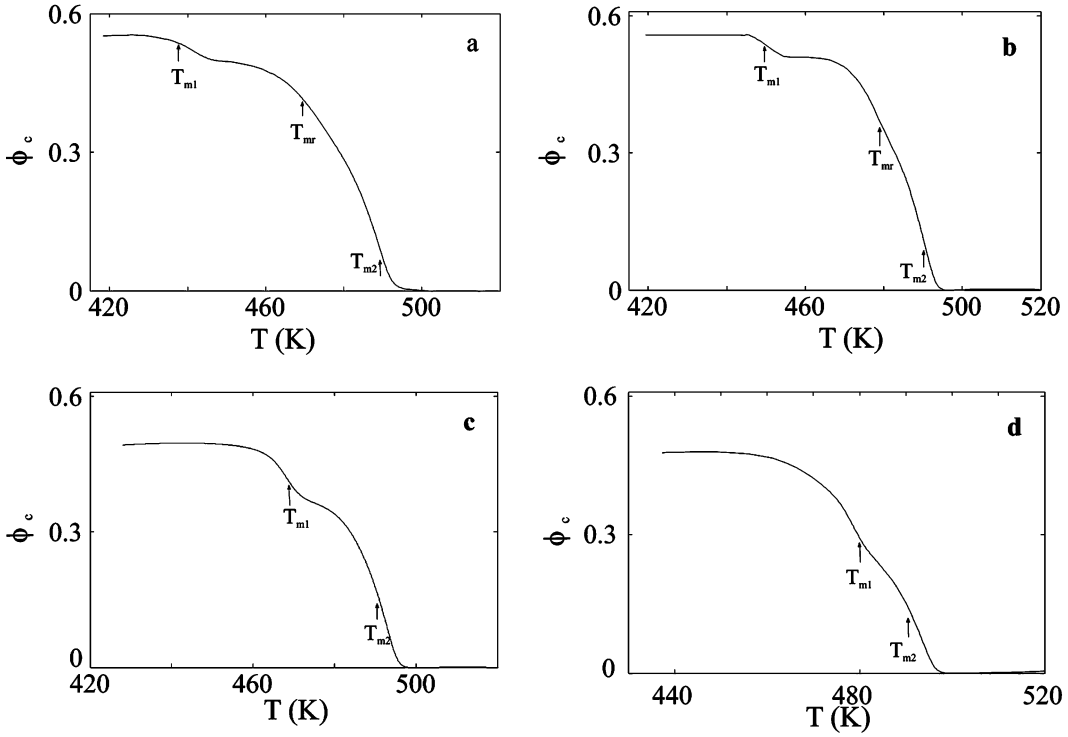

Figure 6. Crystallinity vs temperature T (K) over the melting region for iPS SGC samples crystallized at the indicated temperatures for 2 weeks: (a) 65 °C, melting range 417−520 K; (b) 73 °C, melting range 419−520 K; (c) 100 °C, melting range 428−520 K; (d) 120 °C, melting range 437−520 K.

RAF experiences an irreversible relaxation with small production of enthalpy. This results in the deviation between the total heat capacity and the baseline heat capacity. The treated samples having lower T_g than the original ones suggest that the high glass transition temperature in the original samples is probably due to strong coupling between the poor crystals or RAF and the amorphous phase and is formed during cooling. The RAF is possibly located at the surfaces of the SGC crystals.

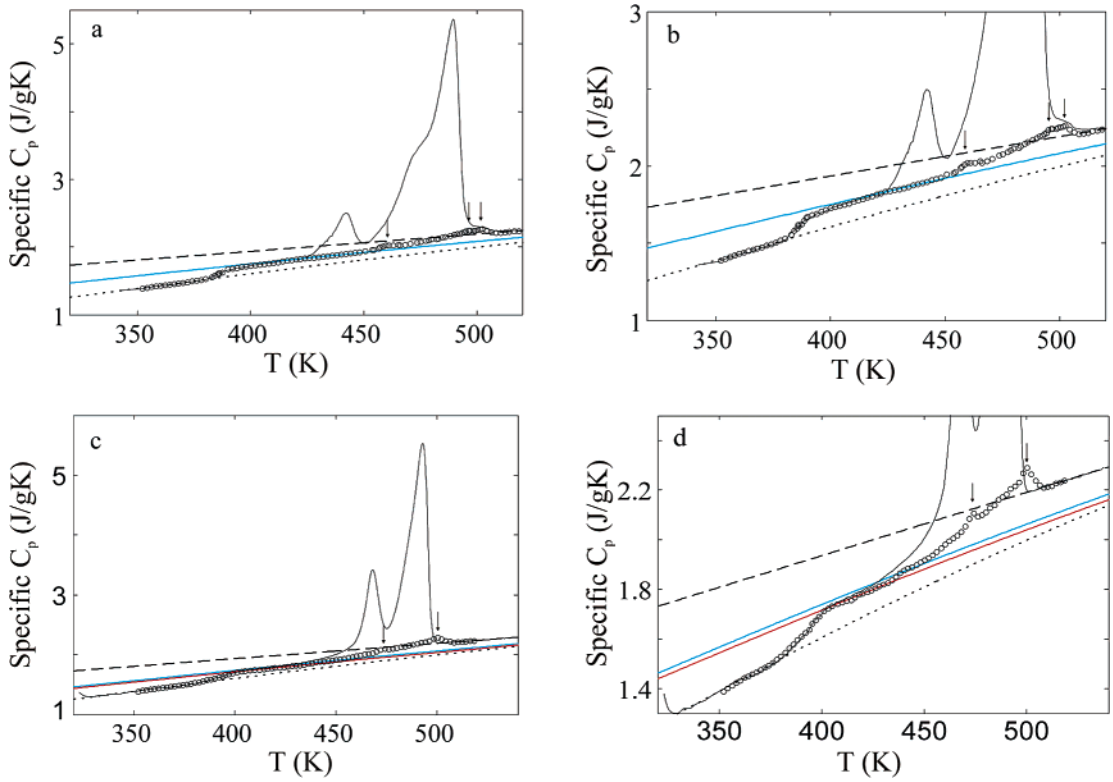

Figure 7. Quasi-isothermal TMDSC specific reversing heat capacity (open circles) and standard DSC specific total heat capacity (solid curve) for iPS SGC samples crystallized for 2 weeks at (a) 65 °C, wide scaling; (b) 65 °C, expanded scaling; (c) 100 °C, wide scaling; (d) 100 °C, expanded scaling. Heat capacity of liquid iPS (dashed line) and solid iPS (dotted line) are obtained from the ATHAS data bank.[30] The solid lines refer to three-phase model (red line) or two-phase model (blue line) with phase fractions listed in Table 2.

Within the melting region, the degree of crystallinity as a function of temperature, $\phi_c(T)$, can be calculated using Euler's method to solve the following equations iteratively:[1,32,33]

$$C_p^{exp}(T) = \phi_c C_p(T)|_{solid} + (1 - \phi_c)C_p(T)|_{liquid} - (d\phi_c/dT)\Delta H_f(T) \quad (5a)$$

$$C_p(T)|_{liquid} - C_p^{exp}(T) = \Delta H_f(T)\,(d\phi_c/dT) + \phi_c(d\Delta H_f(T)/dT) \quad (5b)$$

where $C_p^{exp}(T)$ is the experimentally measured heat capacity and $\Delta H_f(T)$ is the temperature-dependent heat of fusion corrected by the factor $f = 2T/(T + T_m^0)$[34] using the literature value of 515 K (242 °C)[29] as the infinite crystal melting point, T_m^0. We chose to use this value of T_m^0 (rather than our extrapolated value from Figure 3) because it is based on a much larger data set. This choice made no practical difference, the variation being much smaller than the error range of the measurements. The melting range was chosen from the intersection point (marked with blue arrows in Figure 4a–d) between the baseline heat capacity based on the two-phase model (blue solid line in Figure 4a–d) and total specific heat capacity (solid curve in Figure 4a–d) up to absolute melt (520 K). These intersection points are 417 K (144 °C) for T_c = 65 °C (Figure 2a), 419 K (146 °C) for T_c = 73 °C (Figure 2b), 428 K (155 °C) for T_c = 100 °C (Figure 2c), and 437 K (164 °C) for T_c = 120 °C (Figure 2d).

Equation 5b was solved numerically by Euler's method (using Matlab R13). The degree of crystallinity, shown in Table 1 for all SGC samples, prior to melting was used as the starting point for the iterative calculation. Figure 6 shows the temperature-dependent degree of crystallinity for all SGC samples, and the positions of the endotherm peaks are marked in the figure. In Figure 6a,b, after some amount of crystals melts at T_{m1}, the crystallinity maintains a constant level over a small temperature range instead of continuing to decrease with increasing temperature. This suggests there is some immediate reorganization (recrystallization) occurring for the molecules melting at T_{m1}. After the reorganization, the second endotherm T_{mr} appears in samples crystallized at 65 or 73 °C. No T_{mr} was observed for the samples crystallized at 100 and 120 °C. We suggest the endotherm at T_{mr} is the melting of reorganized molecules, which melt at very low temperature at T_{m1}. In Figure 6a–d, all the remaining crystals are melted at the completion of T_{m2}, leaving homogeneous liquid. We remark parenthetically that no other choice of either ϕ_c or the starting point for crystal melting resulted in a satisfactory solution for Euler's equations. This strongly suggests that the RAF relaxes before the crystals begin to melt and, conversely, that no crystals melt prior to the start of the T_{m1} endotherm signaled by the intersection of the two-phase model baseline heat capacity curve and the data curve.

Heat Capacity by Quasi-Isothermal TMDSC. Figure 7 shows the quasi-isothermal TMDSC specific reversing heat capacity (open circles) and the standard DSC specific total heat capacity (solid curve) for the iPS SGC samples crystallized at 65 °C in Figure 7a,b (expanded view) and at 100 °C in Figure 7c,d (expanded view). These two crystallization temperatures were chosen as representatives since the behavior of the SGCs crystallized at 73 °C was similar to 65 °C and the

behavior of the SGCs crystallized at 120 °C was similar to 100 °C. In Figure 7, the heat capacity of iPS solid (dotted line) and the heat capacity of liquid (dashed line) are shown, along with the baseline heat capacity based on the three-phase model (red line) or the baseline heat capacity based on the two-phase model (blue line). The quasi-isothermal measurement (open circles) matches the total heat capacity measurement very well above the melting point of the highest melting crystals and below the glass transition. Above T_g, there is always some mismatch between these two measurements. At temperatures below the lowest endotherm (T_{m1}), the quasi-isothermal specific reversing heat capacity is just little bit lower than the specific total heat capacity curve, seen most clearly for $T_c = 100$ °C shown in Figure 7d. As we mentioned earlier, such a deviation suggests there is some nonreversing contribution in this temperature range due to enthalpy production, causing the mismatch between the specific total heat capacity and the baseline heat capacity.

The iPS SGC samples behave similarly to the iPS bulk crystallized samples,[1] in that the quasi-isothermal reversing heat capacity data (open circles in Figure 6) show multiple peaks. In all SGC samples we observed a small amount of reversing melting contribution to each of the melting peaks. The location of these small reversing melting peaks, in relation to the major endotherms seen in standard DSC scanning, was dependent upon the chosen T_c.

In the major melting region, in the case of $T_c = 100$ °C (Figure 7d), the quasi-isothermal reversing heat capacity (open circles) shows a small amount of reversing melting contribution to each of the two melting peaks. The two tiny maxima, marked with arrows, are each located on the higher temperature side of their associated DSC melting peaks.

A different situation was observed for the SGC samples crystallized at the lower crystallization temperatures. For the sample crystallized at 65 °C (Figure 7b), the lowest and uppermost arrows mark the positions of the reversing heat capacity peaks (open circles). The uppermost reversing heat capacity peak is still located on the higher temperature side of the correspondent total heat capacity melting peak (T_{m2}). However, the lowest reversing heat capacity peak was at much higher temperature than the first endotherm (T_{m1}) seen in the standard DSC scan and is actually located outside of the melting region of T_{m1}. There also is a tiny shoulder below the uppermost peak in the quasi-isothermal TMDSC specific reversing heat capacity data, marked by the middle arrow, which is associated with the shoulder adjacent to T_{m2} in the standard DSC scan. The behavior of SGC sample crystallized at the lower temperature is related to the effect of annealing that occurs during the quasi-isothermal experiment, which will be discussed in the next section.

During the quasi-isothermal experiment, the temperature is modulated by ±0.5 °C about T_0, the base temperature. The highest and lowest temperature reached during oscillation, $T_0 + 0.5$ °C or $T_0 - 0.5$ °C, are still well within the melting peak of the endotherm. Referring to Figure 7c (SGC sample crystallized at 100 °C), the total heat capacity trace (solid curve) shows two positive deflections above 460 K. These reflect the two crystal melting events in the heat flow trace of Figure 7c (solid curve) seen during scanning calorimetry. The full width at half-maximum (fwhm) of the heat capacity

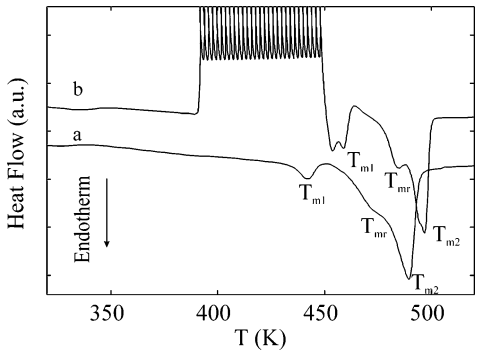

Figure 8. Standard DSC scan (lower curve a) and specialized scan (upper curve b, treatment described in the text) of an iPS SGC sample grown at T_c = 65 °C. Endotherms are presented with downward deflection from the baseline.

peaks gives $\Delta T = 7$ °C for the lower temperature peak and $\Delta T = 10$ °C for the upper temperature peak. Thus, during oscillation about T_0, the temperature stays within the range of crystal melting since the fwhm is 14−20 times greater than the modulation amplitude. The phenomenon of reversing melting has been documented for several flexible chain polymers.[1,6,32,33,35−40] The concept of molecular nucleation introduced by Wunderlich[33,35,36] is used to explain the reversible latent heat contribution in the melting region.[6] The idea of molecular nucleation is that a flexible polymer chain must go through a nucleation step before adding to the growth face of a crystal.[6] The observation of two small reversing melting peaks, associated with the two crystal melting events, is interpreted to imply that the molecular nucleus remains during the cooling cycle but does not trigger any recrystallization of already-melted macromolecules for temperatures within the melting region. Quasi-isothermal TMDSC observations support the view that the macromolecular nucleation is needed in addition to crystal nucleation.[6,33,36]

The iPS SGC samples show analogous behavior to cold-crystallized bulk iPS film[1] in the quasi-isothermal TMDSC measurements. First, the amount of reversing melting is still small compared to the total area of the DSC melting peaks, which is a typical phenomenon in long chain macromolecules.[32,33,35−40] Second, the common explanation regarding reversible melting of macromolecules is that a portion of the molecule remains attached to higher melting crystals and cannot be separated after partial melting. This attached part was found to participate only in the high-temperature end of the melting peak.[32,33,36−40] Such a tight attachment of molecules to the crystals was suggested to be the origin of the locally reversible melting and crystallization.[35,41] Quasi-isothermal studies show that iPS SGC samples exhibit very similar behavior to other polymeric systems;[1,32,33,36−39] thus, the suggestion about a reversible melting mechanism can also apply to our model solution grown crystal system.

Annealing during Quasi-Isothermal Treatment. In Figure 7a,b, we found that the lowest reversing melting peak in the quasi-isothermal measurement is located out of the region of the lowest endotherm seen in the standard DSC scan. This effect may be due to annealing during the quasi-isothermal experiments. To verify this suggestion, we use a quasi-isothermal treatment without temperature modulation, followed immediately by a standard DSC scan. In Figure 8, the lower curve, marked a, gives the standard DSC scan of

original SGC sample crystallized at 65 °C with heating rate of 10 K/min. The upper curve, marked b, is a specialized scan of iPS SGC sample grown at 65 °C and then treated in the DSC cell with the following sequence: (1) The sample is first heated to 390 K (117 °C) at 10 K/min. (2) The sample is held isothermally for 20 min, and then the temperature is increased by 2 K. (3) Step 2 is repeated until the temperature reaches 450 K (177 °C), and then the sample is heated to melting at 10 K/min. Except for modulation, step 2 replicates the annealing that would occur in the quasi-isothermal experiment.

As shown in Figure 8, the endotherms (T_{m1}, T_{mr}, and T_{m2}) in the upper curve b are all located at higher temperatures than in the lower curve a. (Endotherms are presented with downward deflection. The endothermic event just below T_{m1} in curve b is an artifact due to DSC system equilibration effect.) The shift of the endothermic peaks to higher temperature is clear evidence of annealing of the crystals. The quasi-isothermal process anneals the existing crystals, causing the melting points to be shifted to higher temperatures. Thus, we can understand why the lowest reversing melting peak in the quasi-isothermal measurements does not correspond to the lowest endotherm (T_{m1}) in the original DSC scan and why the upper reversing melting peak occurred partially outside the melting range of the highest endotherm (T_{m2}) in the original DSC scan. At slow heating rate (as in the quasi-isothermal experiment), the crystals of lower and higher stability can be annealed to become more perfect and more stable and therefore melt at higher temperature.

Discussion

Our previous work used standard DSC and quasi-isothermal TMDSC on cold-crystallized iPS bulk film.[1] Three endothermic events were observed in standard DSC; the lowest of these was not a crystal endotherm but was instead the relaxation of the relatively large fraction of RAF ($\phi_{RAF} = 0.10-0.12$). In the iPS bulk film, the RAF relaxed below the melting point of the crystals and formed an enthalpic peak.[1] The iPS SGC samples studied in the present work also display multiple endothermic events in standard DSC. The difference is that the lowest endotherm is truly the melting of portions of crystal lamellae, i.e., the melting of the least thermally stable portions. The very small amounts of RAF reported here (0.01−0.03) relax over a wide range of temperatures and do not show an enthalpic peak. The signature of the RAF relaxation in SGC samples is the observation of the excess heat capacity between T_g and T_{m1}.

The quasi-isothermal heat capacity studies of iPS SGCs show an important similarity to the same studies[1] conducted on iPS bulk film. In both cases, multiple reversing melting peaks are seen, and iPS is the first such polymer to show this behavior. Other polymers showing dual melting peaks in standard DSC scans, such as poly(ethylene terephthalate)[36] and poly[carbonyl(ethylene-*co*-propylene)],[32] possessed only a single peak in the quasi-isothermal measurements. There is only one other reported case of multiple reversing melting peaks and that involved a low molecular mass oligomer (1500 Da) of poly(oxyethylene).[37] In that work, the dual reversing melting was attributed to melting of different molecular populations with different molecular weights.

Dual reversing melting endotherms have been observed in polymeric material, so far only in iPS, either in cold-crystallized films[1] or in SGC's. The reason that iPS behaves in this manner may be related to Petermann's[2] previous proposal regarding the observation of multiple melting of iPS by standard DSC. Petermann[2] suggested that the origin of multiple melting of iPS is due to a nonuniform thermal stability distribution along one single lamella, possibly due to uneven tacticity distribution. By using TEM, Petermann[2] observed that an individual lamella became broken when the temperature reached T_{m1}, and the remaining parts of the lamella became completely melted after $T = T_{m2}$. In between, reorganization was observed, and the broken lamella was "repaired". From our quasi-isothermal studies of iPS bulk films, we find that the lowest reversing melting peak in quasi-isothermal measurements is associated with the melting of portions of the lamellae with low stability, and the uppermost one corresponds to the remaining portions of lamellae with high thermal stability.[1] Similarly, we believe this model also could be applied to interpret the melting behavior of iPS SGCs since the SGC model system demonstrates almost the same features in melting region, despite the supposition that the SGC lamellae possibly are larger in two dimensions. We are currently investigating the morphology and structure of iPS SGCs using small-angle X-ray scattering and electron microscopy.

The effect of reorganization or annealing is also investigated in this study. During a standard DSC scan, cold-crystallized bulk iPS film showed an obvious recrystallization exotherm just above the first crystal melting point[1] (seen in Figure 2e). The heat capacity showed a strong negative departure from the liquid (melt) baseline, between T_{m1} and T_{m2}. In contrast, in the SGC samples, we observe such recrystallization/reorganization only for samples crystallized at the lower temperatures. In Figure 6a,b, the crystalline fraction can be seen to flatten (Figure 6a, $T_c = 65$ °C) or slightly increase (Figure 6b, $T_c = 73$ °C) at about 465 K (192 °C). On the time scale of the standard DSC scan at heating rate of 10 °C/min the SGC samples crystallized at 100 or 120 °C do not show explicit reorganization, although in the quasi-isothermal experiments, with heating rate $q \rightarrow 0$, all SGCs show the effects of annealing. The melting points T_{m1}, T_{mr}, and T_{m2} all increase after prolonged annealing treatment, which could explain why the reversing melting peaks in quasi-isothermal TMDSC experiments are located at the higher temperature side of correspondent melting peaks observed in standard DSC scan. In our recent study using real-time small-angle X-ray scattering, we propose a model of crystal lamellae melting of iPS bulk films by taking the annealing effect into account explicitly.[42] The validity of this model for iPS SGC's needs further investigation.

Conclusion

IPS crystals were grown from dilute solutions in dimethyl phthalate over a wide range of crystallization temperatures to serve as model materials for thermal studies. Thermal analysis was carried out to determine the temperature-dependent heat capacity, $C_p(T)$, using standard DSC and quasi-isothermal TMDSC. Compared to heat capacity studies of iPS bulk films reported earlier,[1] the SGCs show some important differences. The iPS SGCs have higher degrees of crystallinity, and much

lower rigid amorphous fractions, compared to cold-crystallized iPS bulk film. Unlike the bulk iPS film, the RAF in SGCs does not show an enthalpic relaxation peak. Instead, the RAF in SGCs relaxes over a broad range of temperatures from just about the glass transition of the MAF to just below the first melting endotherm. Two or three endotherms are observed in standard DSC scanning of iPS SGCs, dependent upon the crystallization temperature. Lower temperature crystallization (65 or 73 °C) results in less stable crystals that reorganize during DSC scanning. These crystals melt again to form the shoulder at T_{mr} on the low-temperature side of the major melting endotherm.

Despite these differences, there are some important similarities between the thermal behavior of iPS SGCs and iPS bulk film. The quasi-isothermal TMDSC results show that there are multiple reversing melting endotherms observed for all iPS SGC samples. Prior quasi-isothermal studies of bulk cold-crystallized iPS also showed dual reversing melting peaks. Each small reversing melting peak, in either iPS bulk or SGCs, is suggested to be associated with the melting of a different portion along the lamella, consistent with TEM observations of Petermann.[2] The reversing melting peak is always located on the higher temperature side of its corresponding melting peak, suggesting that the most stable remaining crystals contain the molecules that reversibly melt.

We studied the effects of annealing on the thermal properties of iPS SGCs. Here we distinguish the behavior of the SGCs crystallized at lower temperatures (65 or 73 °C). We observe that the lowest temperature reversing melting peak seen in quasi-isothermal measurements is upshifted so that it occurs at a temperature completely outside the range of the lowest endotherm of the standard DSC scan. The highest temperature reversing melting peak also is upshifted, although there is some overlap with its associated DSC endotherm. This behavior is attributed to annealing of the crystals during the quasi-isothermal heating.

Both standard DSC and quasi-isothermal TMDSC results show that iPS SGC samples grown at low temperatures have lower stability (reduced crystal perfection), and therefore annealing and reorganization occur during heating. Annealing especially occurs under the slow heating rate conditions used in quasi-isothermal TMDSC and leads to the complete mismatch between the temperature location of the reversing melting peak in quasi-isothermal TMDSC experiment ($q \rightarrow 0$) and the melting peak in standard DSC scan (relatively high $q = 10$ °C/min). Morphological studies (by atomic force microscopy and scanning electron microscopy) and structural studies (by real-time small-angle X-ray scattering) are presently underway to ascertain the origin of the differences between the iPS SGCs grown at lower and higher crystallization temperatures.

Acknowledgment. The National Science Foundation, Division of Materials Research, Polymers Program, supported this research through Grant DMR-0100646.

References and Notes

(1) Xu, H.; Cebe, P. *Macromolecules* **2004**, *37*, 2797.
(2) Liu, T.; Petermann, J. *Polymer* **2001**, *42*, 6453.
(3) Mandelkern, L.; Alamo, R. G.; Kennedy, M. A. *Macromolecules* **1990**, *23*, 3, 4721.
(4) Xu, H.; Ince, B. S.; Cebe, P. *J. Polym. Sci., Part B: Polym. Phys.* **2003**, *41*, 3026.
(5) Natesan, B.; Xu, H.; Ince, B. S.; Cebe, P. *J. Polym. Sci., Part B: Polym. Phys.* **2004**, *42*, 777.
(6) Wunderlich, B. *Prog. Polym. Sci.* **2003**, *28*, 383.
(7) Song, M. J. *Appl. Polym. Sci.* **2001**, *81*, 2779.
(8) Cheng, S. Z. D.; Pan, R.; Wunderlich, B. *Makromol. Chem.* **1988**, *189*, 2443.
(9) Huo, P. P.; Cebe, P. *Macromolecules* **1992**, *25*, 902.
(10) Cheng, S. Z. D.; Cao, M. Y.; Wunderlich, B. *Macromolecules* **1986**, *19*, 1868.
(11) Huo, P.; Cebe, P. *Colloid Polym. Sci.* **1992**, *270*, 840.
(12) Lu, S. X.; Cebe, P. *Polymer* **1996**, *37*, 4857.
(13) Schick, C.; Wurm, A.; Mohammed, A. *Thermochim. Acta* **2003**, *396*, 119.
(14) Blais, P.; Manley, R. S. J. *J. Polym. Sci., Polym. Polym. Phys. Ed.* **1966**, *4*, 1022.
(15) Keith, H. D.; Vadimsky, R. G.; Padden, F. J. *J. Polym. Sci., Part B: Polym. Phys.* **1970**, *8*, 1687.
(16) Sasaki, T.; Kurita, M.; Yabu, T.; Takahashi, T. *Macromolecules* **1995**, *28*, 8528.
(17) Kramers, H. A. *Physica* **1940**, *7*, 284.
(18) Hanggi, P.; Talkner, P.; Borkovec, M. *Rev. Mod. Phys.* **1990**, *62*, 251.
(19) Brandup, J.; Immergut, E. H.; Grulke, E. A.; Abe, A.; Bloch, D. R. *Polymer Handbook*; Wiley-Interscience; New York, 1999.
(20) Suzuki, H.; Grebowicz, J.; Wunderlich, B. *Br. Polym. J.* **1985**, *17*, 1.
(21) Ishikiriyama, K.; Wunderlich, B. J. *Thermal. Anal.* **1997**, *50*, 337.
(22) Kimura, T.; Ezure, H.; Tanaka, S.; Ito, E. *J. Polym. Sci., Part B: Polym. Phys.* **1998**, *36*, 1227.
(23) Kobayashi, M.; Tsummura, K.; Tadokoro, H. *J. Polym. Sci., Part B: Polym. Phys.* **1968**, *6*, 1493.
(24) Kobayashi, M.; Akita, K.; Tadokoro, H. *Makromol. Chem.* **1968**, *118*, 324.
(25) Painter, P. C.; Koeing, J. L. *J. Polym. Sci., Part B: Polym. Phys.* **1977**, *15*, 1885.
(26) Kobayashi, M.; Nakaoki, T. *Macromolecules* **1990**, *23*, 78.
(27) Gu, F. M.; Bao, L. R.; Chen, M.; Bu, H. S. *Macromol. Rapid Commun.* **1998**, *19*, 367.
(28) Nakoaki, T.; Kobayashi, M. *J. Mol. Struct.* **1991**, *242*, 315.
(29) Lemstra, P. J.; Kooistra, T.; Challa, G. *J. Polym. Sci., Part B: Polym. Phys.* **1972**, *10*, 823.
(30) ATHAS data bank, http://web.utk.edu/~athas/databank/, Ed.; M. Pyda, 1994.
(31) Wunderlich, B. *Thermochim. Acta* **2003**, *403*, 1.
(32) Pyda, M.; Di Lorenzo, M.; Pak, J.; Kamasa, P.; Buzin, A.; Grebowicz, J.; Wunderlich, B. *J. Polym. Sci., Part B: Polym. Phys.*, **2001**, *39*, 1565.
(33) Di Lorenzo, M.; Pyda, M.; Wunderlich, B. *J. Polym. Sci., Part B: Polym. Phys.* **2001**, *39*, 1594.
(34) Hoffman, J. D.; Davis, G. T.; Lauritzen, J. I. In *Treatise on Solid State Chemistry*; Haney, N. B., Ed.; Plenum Press: New York, 1976.
(35) Wunderlich, B.; Mehta, A. *J. Polym. Sci., Part B: Polym. Phys.* **1974**, *12*, 255.
(36) Okazaki, I.; Wunderlich, B. *Macromolecules* **1997**, *30*, 1758.
(37) Ishikiriyama, K.; Wunderlich, B. *Macromolecules* **1997**, *30*, 4126.
(38) Wurm, A.; Merzlyakov, M.; Schick, C. *Colloid Polym. Sci.* **1998**, *276*, 289.
(39) Androsch, R.; Wunderlich, B. *Macromolecules* **2001**, *34*, 5950.
(40) Okazaki, I.; Wunderlich, B. *Macromol. Rapid Commun.* **1997**, *18*, 313.
(41) Mehta, A.; Wunderlich, B. *Macromol. Chem.* **1974**, *175*, 977.
(42) Xu, H.; Cebe, P. *Polymer*, in press.

MA048042L